



Contents lists available at ScienceDirect

Ore Geology Reviewsjournal homepage: www.elsevier.com/locate/oregeo

Late Triassic E-MORB-like basalts associated with porphyry Cu-deposits in the southern Yidun continental arc, eastern Tibet: Evidence of slab-tear during subduction?

JianLin Chen ^{a,b,*}, JiFeng Xu ^{a,b}, JiangBo Ren ^c, XiaoXiao Huang ^a^a State Key Laboratory of Isotope Geochemistry, Guangzhou Institute of Geochemistry, Chinese Academy of Sciences, Guangzhou 510640, China^b CAS Center for Excellence in Tibetan Plateau Earth Sciences, Beijing 100101, China^c Guangzhou Marine Geological Survey, Guangzhou 510075, China**ARTICLE INFO****Article history:**

Received 25 April 2016

Received in revised form 24 October 2016

Accepted 12 December 2016

Available online 23 December 2016

Keywords:

Basalt

Slab-tear

Porphyry Cu deposit

Southern Yidun arc

Eastern Tibet

ABSTRACT

It is generally believed that andesite–dacite–rhyolite suites and contemporary porphyry Cu deposits are related to subduction in active continental margin settings. However, it is still unclear which tectonic events result in the generation of porphyry Cu deposits and whether asthenospheric mantle material is involved in this process. Widespread andesitic–dacitic felsic intrusions associated with porphyry Cu deposits and rarer basalts have been identified in the Late Triassic southern Yidun arc (SYA) of eastern Tibet. However, few geochronological and geochemical data are available for these basalts, thereby hampering the development of geodynamic models for this magmatic event and the formation of related porphyry Cu deposits in the region. Here we present the first geochemical and SIMS (secondary ion mass spectrometry) zircon U–Pb data of Xiaoxiaoliu basalts in the SYA. The age of the Late Triassic Xiaoxiaoliu basalts (216.1 ± 2.8 Ma) is consistent with the timing of emplacement of voluminous porphyritic intrusions and the formation of Cu deposits within the SYA (peaking at 215–217 Ma). The Xiaoxiaoliu basalts have E-MORB-like trace element patterns that are free of negative Nb–Ta anomalies, and have high $^{143}\text{Nd}/^{144}\text{Nd}_{\text{t}}$ values, suggesting they were sourced from asthenospheric mantle without any arc-type influence. These observations, combined with the fact that some Late Triassic mineralized porphyritic intrusions within the SYA have adakitic affinities, suggest that the basalts and other igneous rocks and associated porphyry Cu deposits within the SYA were produced by tearing of a westward-dipping slab, triggering the upwelling of asthenospheric mantle material during subduction of the Garze–Litang Ocean crust.

© 2016 Published by Elsevier B.V.

1. Introduction

Andesite–dacite–rhyolite suites and porphyry Cu deposits often occur in active continental margin settings (e.g., the Andes in South America) and are thought to relate to thermal-perturbation-induced melting of lithospheric mantle material (e.g., Houseman et al., 1981; Davies and von Blankenburg, 1995). However, the generation of porphyry Cu deposits only occurs during a few specific and ephemeral tectonic events during subduction (e.g., Kay and Mpodozis, 2001). In addition, it is unusual to find asthenospheric-mantle-derived basaltic magmas in continental arc settings. Here, we present new geochemical and SIMS U–Pb

zircon age data for E-MORB-like basalts that were most likely derived from asthenospheric mantle within the southern Yidun arc (SYA) of the eastern Tibetan Plateau. This area contains widespread Late Triassic arc-related igneous rocks and porphyry Cu deposits (Deng et al., 2014; Wang et al., 2014; Hou and Zhang, 2015; Zu et al., 2016), as exemplified by the Pulang Cu deposit, one of the largest porphyry Cu deposits in China. We suggest the E-MORB-like basalts and associated porphyry Cu deposits in SYA were produced by slab-tear during subduction.

2. Geological background

The north–south trending Yidun continental arc (or Yidun arc) is located in eastern Tibet, and is separated from the Yangtze Craton to the east by the Garze–Litang suture, and from the Zhongza block to the west by the Xiangcheng–Geza Fault (Roger et al.,

* Corresponding author at: State Key Laboratory of Isotope Geochemistry, Guangzhou Institute of Geochemistry, Chinese Academy of Sciences, Guangzhou 510640, China.

E-mail address: ldxchen@gig.ac.cn (J. Chen).

2010; Yang et al., 2012; Fig. 1A and B). It is generally believed that the Garze–Litang suture formed at the end of the Triassic (Reid et al., 2005), and the Yidun arc resulted from westward subduction of Garze–Litang ocean crust in the Late Triassic (Yang et al., 2012). The arc is dominated by Upper Triassic volcanic–sedimentary successions that contain flysch-like sediments and mafic–silicic volcanic arc rocks (BGMRSP, 1991). The subduction-related volcanic rocks in the Yidun arc formed between 245 and 210 Ma (e.g., Wang et al., 2011, 2013; Yang et al., 2012; Chen et al., 2014). The volcanic rocks within the southern part of the Yidun arc (SYA, also called the Zhongdian arc; Fig. 1C) are dominantly sub-alkaline basalts, andesites, and dacites that occur as interlayers within the Qugasi and Tumugou groups. The andesites and basalts in this area are also associated with Late Triassic quartz diorite and quartz monzonite dominated porphyritic intrusions and Cu deposits (e.g., the Pulang porphyry Cu deposits) (Deng et al., 2014; Hou and Zhang, 2015; Zu et al., 2016).

Fresh to moderately altered basalt samples were collected from the Xiaoxiaoliu area ($28^{\circ}01'45''$ – $28^{\circ}02'11''$ N, $99^{\circ}54'05''$ – $99^{\circ}50'47''$ E) of the SYA during this study (Figs. 1C, 2A and B). These basalts discontinuously crop out over a total area of $\sim 2 \text{ km}^2$. All samples obtained during this study are massive, dark gray to gray-green,

and are generally porphyritic, containing euhedral–subhedral plagioclase, pyroxene, and amphibole phenocrysts that form $<10 \text{ vol.\%}$ of the rocks and are hosted by microcrystalline matrix material (Fig. 2B and C). Plagioclase within these units is elongate and columnar, and has undergone partial alteration to sericite and epidote (Fig. 2B and C). The granular pyroxene within these basalts is fractured and has undergone post-magmatic alteration to carbonate and chlorite.

3. Analytical techniques

All samples were cleaned of weathered surfaces prior to being powdered in an agate ring mill for subsequent major and trace element and Sr–Nd isotopic analyses at the Guangzhou Institute of Geochemistry, Chinese Academy of Sciences (GIGCAS), Guangzhou, China.

Major elements were measured by X-ray fluorescence (XRF) spectrometry using fused glass disks and following the analytical procedures described by Goto and Tatsumi (1996). Pre-ignition at 900°C was used to determine loss on ignition (LOI) values prior to major element analyses. The analysis of Chinese standard refer-

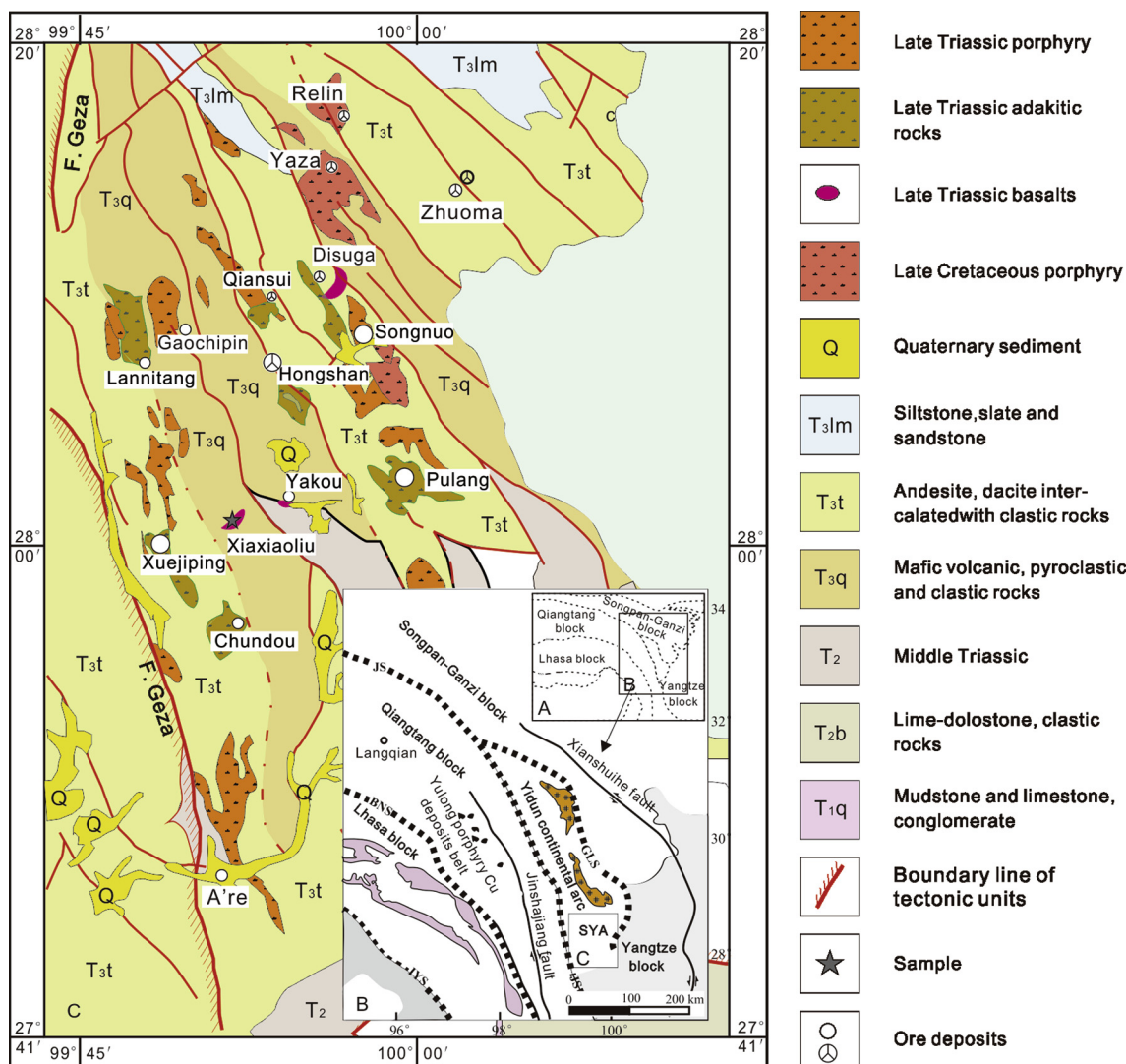


Fig. 1. A) and B) Geological map of the Yidun Block. C) Geological map of the southern Yidun arc region, adapted from Huang (2013) and Chen et al. (2014). Abbreviations are as follows: JS = Jinsha suture, GLS = Garze–Litang suture, BNS = Bangong–Nujiang suture, IYS = Indus–Yalu sutures, F. Geza = Xiangcheng–Geza Fault.

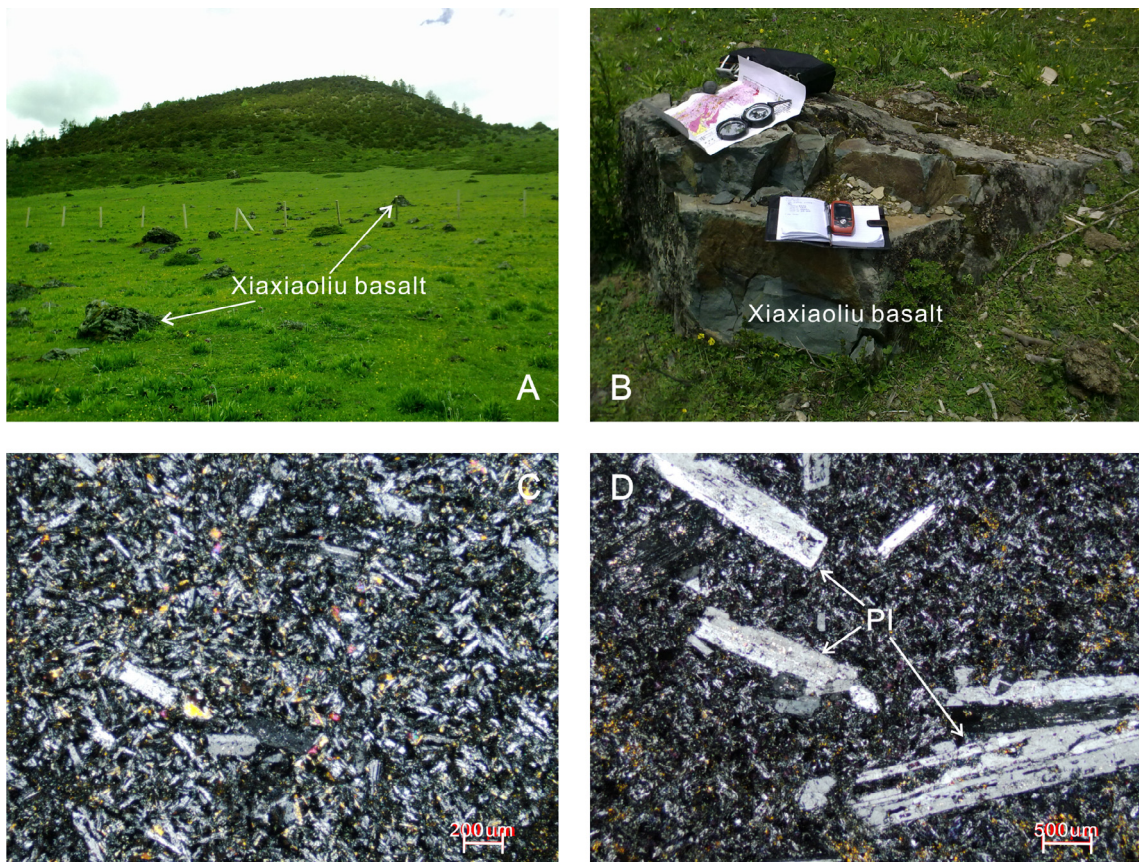


Fig. 2. (A–B) Field photographs of basalt from the Xiaxiaoliu area of the southern Yidun arc. (C–D) Photomicrographs showing representative examples of the Xiaxiaoliu basalts within the southern Yidun arc. Abbreviations are as follows: Pl = plagioclase.

ence materials GSR-1, GSR-2, and GSR-3 yielded major element analytical uncertainties that were generally better than 5%. Trace element compositions were determined using inductively coupled plasma–mass spectrometry (ICP–MS), following the analytical procedures described by Chen et al. (2010). The precision of the rare earth element (REE) and high field strength element (HFSE) analyses study is estimated to be 5%.

Sr and Nd isotopic compositions were measured using thermal ionization mass spectrometry (TIMS) employing a Triton instrument at GIGCAS and following the analytical procedures described in detail by Li et al. (2004), Wei et al. (2002), and Chen et al. (2010). The method of chemical separation of Sr and Nd was similar to that described by Li and McCulloch (1998), Xu et al. (2002), and Chen et al. (2010). The $^{87}\text{Sr}/^{86}\text{Sr}$ value of the NBS987 standard and the $^{143}\text{Nd}/^{144}\text{Nd}$ value of the JNdI-1 standard were 0.710288 ± 28 (2σ) and 0.512109 ± 12 (2σ), respectively, with fractionation corrections of $^{146}\text{Nd}/^{144}\text{Nd} = 0.7219$ and $^{86}\text{Sr}/^{88}\text{Sr} = 0.1194$ applied to all measured $^{143}\text{Nd}/^{144}\text{Nd}$ and $^{86}\text{Sr}/^{88}\text{Sr}$ values, respectively.

Samples for U–Pb analysis were processed by conventional magnetic and density techniques to concentrate the non-magnetic heavy fraction. The resulting zircon separates were mounted with a 91500 standard zircon in epoxy mounts that were then polished to expose zircon cross-sections for analysis. All zircons were examined under transmitted and reflected light as well by cathodoluminescence (CL) imaging to examine morphology and internal structures. The grain mounts were then vacuum-coated with high-purity gold prior to analysis by secondary ion mass spectrometry (SIMS), where U, Th, and Pb measurements were undertaken using a Cameca IMS-1280 SIMS instrument at the Institute of Geology and Geophysics, Chinese Academy of Sciences, Beijing, China. U–Th–Pb ratios and absolute abundances were determined

relative to those of a 91500 standard zircon (Wiedenbeck et al., 1995), which was analyzed intermittently during analysis of the unknown zircons. These analyses used operating and data processing procedures similar to those described by Li et al. (2009), employing a mass resolution of 5400 to measure Pb/Pb and Pb/U ratios. A long-term uncertainty of 1.5% (1 RSD) for the $^{206}\text{Pb}/^{238}\text{U}$ measurements of the standard zircons was propagated to the unknowns (Li et al., 2010) despite the fact that the measured $^{206}\text{Pb}/^{238}\text{U}$ error during a specific session was generally around 1% (i.e., 1 RSD) or less. The measured compositions were corrected for common Pb using non-radiogenic common Pb and non-radiogenic ^{204}Pb . These corrections were sufficiently small to be sensitive to the choice of common Pb composition, meaning that an average present-day crustal composition (Stacey and Kramers, 1975) was used for common Pb, assuming that the common Pb encountered during analysis was generally surface contamination introduced during sample preparation. Uncertainties on individual analysis are reported at the 1σ level, with mean ages for pooled U/Pb (and Pb/Pb) analyses quoted at the 95% confidence level. Reduction of the SIMS data was undertaken using the program Isoplot/E v. 2.49 (Ludwig, 2001).

4. Age data and geochemistry

The results of the SIMS zircon U–Pb, major and trace element geochemical, and Nd–Sr isotopic analyses are given in Tables 1 and 2. The basalts were collected from the Xiaxiaoliu area (Fig. 1C), and their age of formation was unknown prior to this study. The results of SIMS zircon U–Pb dating are summarized in Table 1. All analyses yielding a weighted mean $^{206}\text{Pb}/^{208}\text{Pb}$ age of

Table 1

Results of Secondary Ion Mass Spectrometry (SIMS) analysis of zircons in basalts from Xiaoxiaoliu area in southern Yidun arc, eastern Tibet.

Sample spots	U ppm	Th ppm	Th/U	$^{207}\text{Pb}/^{206}\text{Pb}$	1σ	$^{207}\text{Pb}/^{235}\text{U}$	1σ	$^{206}\text{Pb}/^{238}\text{U}$	1σ	$^{207}\text{Pb}/^{206}\text{Pb}$	1σ	$^{207}\text{Pb}/^{235}\text{U}$	1σ	$^{206}\text{Pb}/^{238}\text{U}$	1σ
11XXL-01-1	548	487	1.12	0.05036	9.43	0.23985	9.59	0.0345	1.73	211.6	205.1	218.3	19.0	218.9	3.7
11XXL-01-2	1088	972	1.12	0.05054	1.64	0.23328	2.33	0.0335	1.66	219.8	37.4	212.9	4.5	212.3	3.5
11XXL-01-3	405	368	1.10	0.05034	1.86	0.22909	2.50	0.0330	1.68	210.6	42.5	209.4	4.7	209.3	3.5
11XXL-01-4	256	381	0.67	0.05063	14.2	0.24241	14.3	0.0347	1.88	224.0	299.1	220.4	28.8	220.0	4.1
11XXL-01-5	781	705	1.11	0.05129	5.91	0.24834	6.14	0.0351	1.67	253.9	130.5	225.2	12.5	222.5	3.7
11XXL-01-6	478	477	1.00	0.04946	2.07	0.23414	2.65	0.0343	1.65	169.5	47.6	213.6	5.1	217.6	3.5
11XXL-01-7	295	376	0.79	0.04999	3.02	0.23277	3.49	0.0338	1.76	194.4	68.7	212.5	6.7	214.1	3.7

Table 2

Geochemical and Sr–Nd isotopic data of basalts from Xiaoxiaoliu area in southern Yidun arc, eastern Tibet.

Sample	10XXL-01	10XXL-08	10XXL-10	10XXL-11	10XXL-17	10XXL-18	11XXL-03
SiO_2	44.53	46.86	47.5	46.31	47.76	45.54	47.25
TiO_2	2.57	2.08	2.06	2.36	2.00	2.42	2.16
Al_2O_3	14.62	14.59	14.39	13.35	14.19	14.13	13.67
Fe_2O_3	18.06	14.82	12.69	15.76	14.22	14.74	17.05
MnO	0.22	0.21	0.19	0.25	0.15	0.21	0.24
MgO	5.89	5.75	7.52	6.65	3.74	6.96	5.74
CaO	7.06	9.80	7.57	9.33	7.95	10.03	8.14
Na_2O	3.25	2.47	4.34	2.91	2.53	2.30	4.28
K_2O	0.03	0.04	0.18	0.07	1.70	0.14	0.05
P_2O_5	0.27	0.25	0.22	0.28	0.24	0.23	0.26
LOI	3.13	2.7	2.93	2.31	5.3	2.89	2.16
Mg#	39	44	54	46	34	49	40
Sc	43.9	34.9	45.1	39.3	39.6	40.5	46.6
V	449	379	361	396	309	394	455
Cr	92.8	115	51.1	116	69.5	62.0	71.6
Co	55.8	48.3	51.0	53.4	43.9	52.3	58.4
Ni	74.0	73.6	62.3	80.2	58.3	60.1	72.2
Cu	232	200	186	62.0	55.0	122	259
Zn	121	103	89.0	133	89.9	104	128
Rb	1.24	0.90	1.95	2.62	33.4	1.73	0.88
Ba	35.5	53.2	135	56.1	290	52.1	67.9
Th	1.52	1.44	0.89	1.72	1.11	1.23	1.73
U	0.36	0.28	0.23	0.27	0.34	0.28	0.35
Nb	14.7	14.0	13.1	16.3	14.4	19.5	14.6
Ta	1.04	0.93	0.83	1.10	0.94	1.27	0.90
Pb	4.56	3.56	1.06	9.84	1.29	1.91	1.08
Sr	462	435	199	653	126	170	402
Zr	154	127	122	143	119	148	157
Hf	4.24	3.41	3.33	3.86	3.27	4.06	4.13
Ti	15,405	12,467	12,348	14,146	11,988	14,505	16,184
La	14.7	14.8	10.9	16.3	11.6	12.0	19.4
Ce	33.6	31.9	25.2	35.9	27.3	28.5	41.1
Pr	4.93	4.49	3.72	5.14	3.90	4.20	5.54
Nd	22.3	19.8	17.4	22.7	17.5	19.6	26.0
Sm	5.95	5.10	4.86	5.83	4.88	5.33	6.38
Eu	2.03	1.76	1.75	1.95	1.81	1.86	2.19
Gd	6.52	5.51	5.47	6.34	5.39	5.98	7.46
Tb	1.12	0.93	0.98	1.10	0.95	1.06	1.22
Dy	6.85	5.76	6.18	6.79	6.01	6.65	7.37
Y	34.5	29.6	31.5	34.0	29.1	34.0	34.6
Ho	1.41	1.20	1.29	1.41	1.25	1.39	1.58
Er	3.72	3.21	3.43	3.77	3.32	3.76	4.01
Tm	0.53	0.45	0.50	0.53	0.48	0.53	0.57
Yb	3.28	2.80	3.08	3.32	3.02	3.30	3.26
Lu	0.49	0.43	0.47	0.51	0.46	0.52	0.55
Zr/Nb	10.5	9.07	9.31	8.77	8.26	7.59	10.75
Y/Nb	2.35	2.11	2.40	2.09	2.02	1.74	2.37
La/Sm	2.49	2.90	2.22	2.81	2.37	2.26	3.03
Sm/Yb	1.80	1.82	1.59	1.75	1.62	1.61	1.96
Nb/U	40.8	50.0	57.0	60.4	42.4	69.6	41.7
Th/Ce	0.045	0.044	0.036	0.047	0.040	0.042	0.041
La/Nb	1.00	1.06	0.83	1.00	0.81	0.62	1.33
Ta/La	0.07	0.06	0.08	0.07	0.08	0.11	0.05
$^{87}\text{Sr}/^{86}\text{Sr}$	0.706243	0.704950	0.705604	0.705955	0.706074	0.704596	0.706193
$\pm 2\sigma$	0.000009	0.000009	0.000005	0.000003	0.000006	0.000006	0.000003
$(^{87}\text{Sr}/^{86}\text{Sr})_t$	0.706219	0.704931	0.705517	0.705920	0.703729	0.704505	0.706174
$^{143}\text{Nd}/^{144}\text{Nd}$	0.512917	0.512891	0.512951	0.512891	0.512921	0.512873	0.512841
$\pm 2\sigma$	0.000009	0.000007	0.000009	0.000008	0.000008	0.000007	0.000007
$(^{143}\text{Nd}/^{144}\text{Nd})_t$	0.512689	0.512671	0.512712	0.512672	0.512683	0.512640	0.512631
$\epsilon_{\text{Nd(t)}}$	6.43	6.08	6.87	6.09	6.31	5.47	5.3
$T_{\text{DM}}(\text{Ga})$	0.68	0.68	0.69	0.68	0.78	0.87	0.72

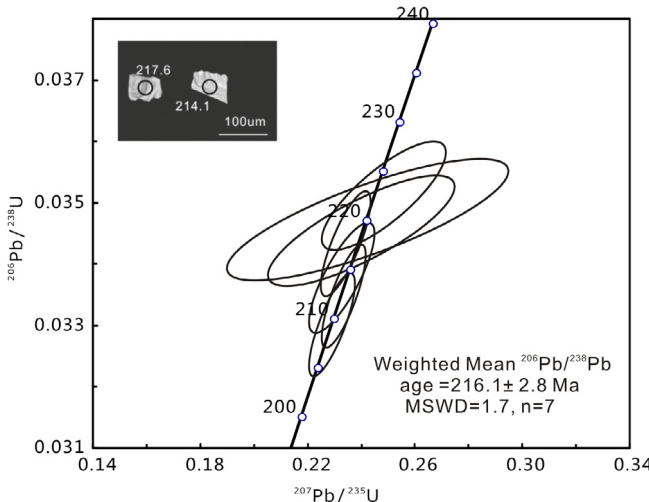


Fig. 3. Secondary ion mass spectrometry (SIMS) U-Pb zircon concordia diagrams for the Xiaxiaoliu basalts of the southern Yidun arc. The inset shows a typical CL image of the zircons analyzed during this study.

216.1 ± 2.8 Ma (Fig. 3). This Late Triassic age is consistent with the timing of the extensive porphyritic intrusions within the SYA, the majority of which formed between 221 and 211 Ma, with peak magmatism at 217–215 Ma (e.g., Chen et al., 2014).

The Xiaxiaoliu basalts have fairly uniform SiO₂ (44.5–47.8 wt%), Fe₂O₃ (12.7–18.1 wt%), MgO (3.7–7.5 wt%), and Al₂O₃ (13.4–14.62 wt%) concentrations, and contain significant amounts of TiO₂ (2.0–2.6 wt%; Table 2). They are classified as low-K and sub-alkaline in a Nb/Y vs. Zr/TiO₂ diagram (Fig. 4A), and record a distinct increase in Ti with increasing differentiation, as exemplified by variations in Zr concentrations, a feature that is indicative of a tholeiitic affinity. The Xiaxiaoliu basalts are geochemically similar to typical E-MORB compositions rather than N-MORB or OIB (Sun and McDonough, 1989); this holds true for the majority of elements barring the heavy REE (HREE). These samples have primitive-mantle-normalized multi-element variation patterns that are free of negative Nb and Ta anomalies and are more fractionated than E-MORB compositions (Fig. 4B). The Xiaxiaoliu basalts also plot closer to E-MORB compositions than to N-MORB or OIB in a Th/Yb vs. Nb/Yb diagram (Fig. 5A). In addition, the low Zr/Nb (7.6–10.8), Y/Nb (1.7–2.4), La/Sm (2.2–3.0), Sm/Yb (1.8–2.0), and La/Yb (3.5–6.0) ratios of the Xiaxiaoliu basalts are

also similar to those of E-MORB compositions (Sun and McDonough, 1989; Table 2; Fig. 5B).

The Xiaxiaoliu basalts have distinctly higher εNd(t) values (5.30–6.87) than the contemporaneous andesite–dacite and felsic intrusions (−1.4 to −5.4) within the SYA (Table 2; Fig. 6). In addition, the former have lower Nd model ages (T_{DM} = 0.68–0.87 Ga, av. 0.73 Ga) than the latter (T_{DM} = 0.98–1.30 Ga, av. 1.16 Ga). The initial Sr isotopic ratios of the Xiaxiaoliu basalts show a wide scatter (Fig. 6), possibly due to the mobility of Rb resulting from seawater alteration.

5. Discussion

5.1. Crustal contamination and fractional crystallization

The Xiaxiaoliu basalts have E-MORB-like geochemical features, such as positive Nb, Ta, P, and Ti anomalies and depleted Nd isotopic compositions, both of which are indicative of negligible crustal contamination. This view is supported by the uniformly high Nb/U (41–70, av. 52) and low Th/Ce (0.036–0.047, av. 0.042) ratios of these samples (Table 2), suggesting that the magmas that formed these basalts assimilated only minor amounts of crustal material prior to emplacement (Condie, 2003).

The low-K Xiaxiaoliu basalts have relatively low MgO (3.7–7.5 wt%), Cr (51–116 ppm), and Ni (58–80 ppm) concentrations, and Mg# values (<54; Mg# = 100 × (MgO/(MgO + FeO_{total})); Table 2) compared with primitive basaltic magmas (Green, 1976), suggesting that the magmas that formed these basalts underwent fractional crystallization prior to eruption or emplacement. In addition, the MgO, Fe₂O₃, TiO₂, Cr, Ni, V, and Co concentrations within these basalts negatively correlate with SiO₂ concentrations, indicating fractionation of olivine, pyroxene, and Fe-Ti oxides. These basalts do not have negative Eu anomalies, suggesting that only minor plagioclase fractionation took place prior to their eruption or emplacement.

5.2. Magma sourcing and petrogenesis

The Xiaxiaoliu basalts have E-MORB-like trace element characteristics and Nd isotopic compositions that require the presence of enriched components in the mantle source, either from the recycling of oceanic crust and various associated continental materials (Schilline, 1973; Willbold and Stracke, 2006; Ulrich et al., 2012; Hofmann, 2014) or as a result of metasomatism (White and

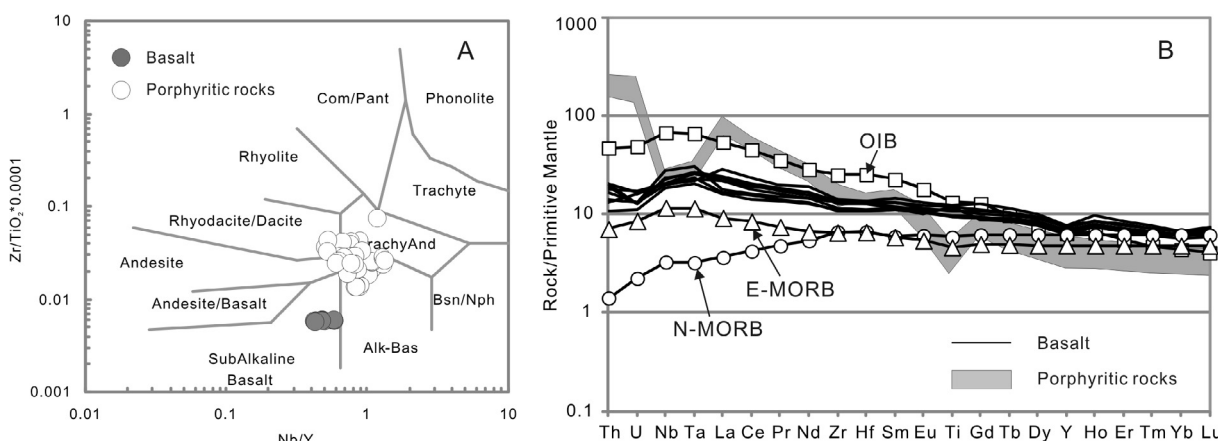


Fig. 4. A) Nb/Y vs. Zr/TiO₂ classification diagram (Winchester and Floyd, 1977) and B) The primitive mantle (PM)-normalized trace element variation diagram for Late Triassic basalts and other igneous rocks within the southern Yidun arc. The primitive mantle composition is from Sun and McDonough (1989), with data from Ren et al. (2011), Wang et al. (2011), Chen et al. (2014), and this study.

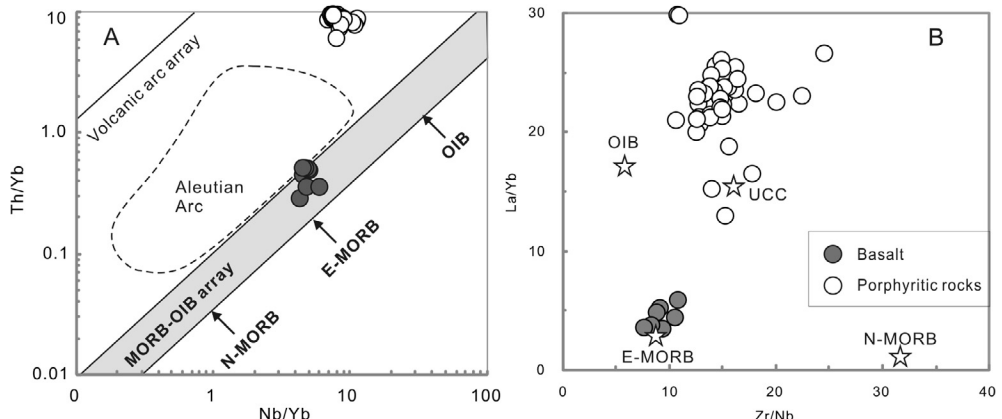


Fig. 5. A) Th/Yb vs. Nb/Yb discrimination diagram for typical oceanic and island arc rocks, showing variations in compositions of samples from the study area (Pearce, 2008). B) Zr/Nb vs. La/Yb diagram showing variations in samples from the study area. Data sources are as follows: normal MORB (N-MORB), enriched MORB (E-MORB), and oceanic-island basalt (OIB) data are from Sun and McDonough (1989); upper continental crust (UCC) values are from Rudnick and Gao (2003); Aleutian arc basalts are from Wan et al. (2012); basalts and other rocks within the southern Yidun arc are from Wang et al. (2011), Chen et al. (2014), and this study.

Hofmann, 1982; Zindler and Hart, 1986; Sun and McDonough, 1989).

Although the Xiaxiaoliu basalts are temporally and spatially associated with arc-affinity andesite–dacite and felsic intrusions within SYA, a significant amount of evidence suggests they formed in an intraplate setting, as follows. (1) Compared with typical arc magmatic rocks with low HFSE contents (e.g., $\text{TiO}_2 < 1 \text{ wt\%}$ and $\text{Nb} < 2 \text{ ppm}$; Martin et al., 2005) and negative Nb-Ta anomalies (Sun and McDonough, 1989), the Xiaxiaoliu basalts do not have negative Nb and Ta anomalies, and contain high concentrations of TiO_2 (2.0–2.6 wt%) and Nb (13.1–19.5 ppm). (2) The Xiaxiaoliu basalts are all classified as intraplate within tectonomagmatic discriminant diagrams, such as Th-Hf/3-Ta ternary (Wood, 1980) and Zr-Zr/Y (Pearce, 1982) diagrams (Fig. 7). (3) The high Nb/U ratios (41–70, av. 52) of the Xiaxiaoliu basalts are consistent with average OIB and MORB compositions (Hofmann, 1997).

The above geochemical features, combined with the low La/Nb (0.62–1.33, av. 0.95) and high Ta/La (0.05–0.11, av. 0.07) ratios of the Xiaxiaoliu basalts (Table 2), suggest that the basalts formed from melts derived from an asthenospheric mantle source (Thompson and Morrison, 1988; Fitton, 1995). In addition, plotting these samples on a $(\text{Sm}/\text{Yb})_N$ vs. $(\text{La}/\text{Sm})_N$ diagram (Fig. 8) indi-

cates that the magmas that formed the Xiaxiaoliu low-K tholeiitic basalts were generated by variable degrees of batch melting (2%–10%) of a hypothetical mantle source containing little garnet ($\text{Cpx:Grt} = 6:1$). In turn, this indicates that the basalts formed at the depth of the spinel-to-garnet transition (<80 km) along the peridotite solidus (McKenzie and O’Nions, 1991; Robinson and Wood, 1998).

The presence of widely distributed Late Triassic andesite–dacite units (including felsic intrusions) and small volumes of basaltic lava within the SYA indicate a genetic link between these two types of magmatism. However, a lack of basaltic andesite in this area and the clearly different geochemical and Nd isotopic characteristics of the basalts and the andesite–dacite units, including the felsic intrusions (e.g., the absence of Nb and Ta depletions and the lower K_2O and Th concentrations, lower Th/Yb, La/Sm, and Sm/Yb ratios, higher $\varepsilon\text{Nd}_{(t)}$ values, and lower Nd model ages of the Xiaxiaoliu E-MORB-like basalts than the andesite–dacite units and the felsic intrusions) suggests these units were derived from different sources (Figs. 5 and 6).

Late Triassic Cu-bearing felsic porphyries, some of which have adakitic affinities, are widely distributed throughout the SYA and are associated with partial melting of the westward subducting Garze–Litang oceanic slab (e.g., Wang et al., 2011; Chen et al., 2014). Slab melting requires anomalously hot slab temperatures that are associated with (1) the subduction of a young and hot oceanic plate (Defant and Drummond, 1990), (2) highly oblique slab subduction (Kelemen et al., 2003), or (3) subduction involving the edge of a torn slab (Yogodzinski et al., 2001). However, the magmatism within the SYA did not involve the subduction of a young oceanic slab, primarily as seafloor spreading within the Garze–Litang Ocean occurred during the Permian (e.g., Yan et al., 2005). In addition, Hou et al. (2004) argued that the back-arc basins and related magmatism within the SYA developed under compression as a result of the low angle of subduction that prevailed during the Triassic, which suggests that the adakitic rocks are not related to highly oblique slab subduction. The new data presented in this study suggest that the adakitic rocks related to porphyry Cu deposits within the SYA were generated by partial melting of the edge of a torn slab involved in westward-dipping subduction of the Garze–Litang Ocean crust. The geochemistry of the Xiaxiaoliu basalts records a minor subduction influence that, when combined with derivation from mantle material within the transitional zone between the stability fields of spinel and garnet, suggests these basalts formed from magmas generated by partial melting of an asthenospheric mantle source underlying

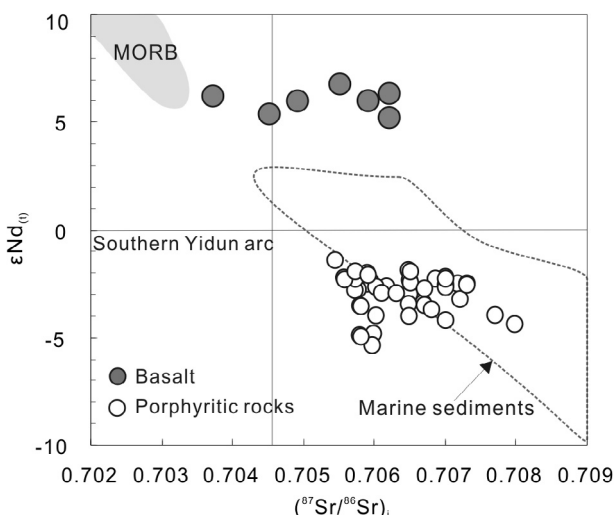


Fig. 6. Sr–Nd isotope compositions of samples from the study area. Marine sediment data are from Plank and Langmuir (1998); all other data sources are as in Fig. 5.

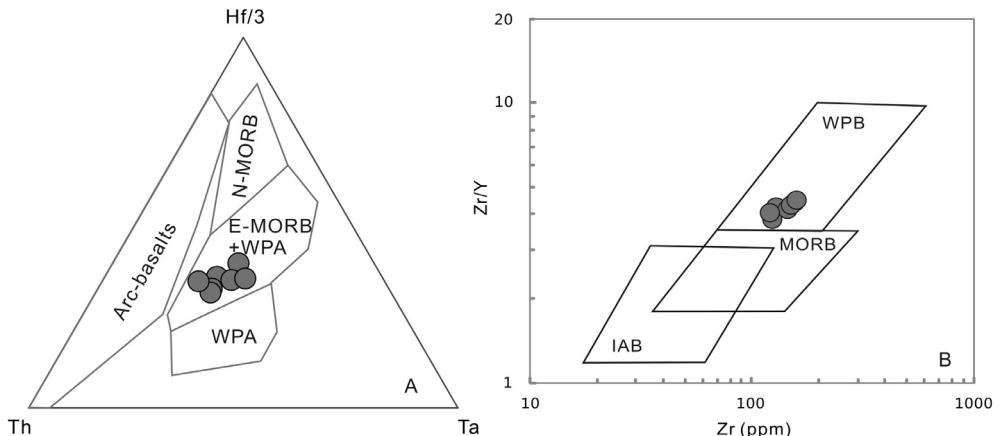


Fig. 7. A) Hf/3-Th-Ta (Wood, 1980) and B) Zr-Y-Zr/γ (Pearce, 1982) tectonomagnetic discriminant diagrams showing variations in the composition of the Xiaoxiaoliu basalts. Abbreviations are as follows: WPT = within-plate tholeiite, WPA = within-plate alkaline basalt, WPB = within-plate basalt, IAB = island arc basalt. Data sources and symbols are as in Fig. 5.

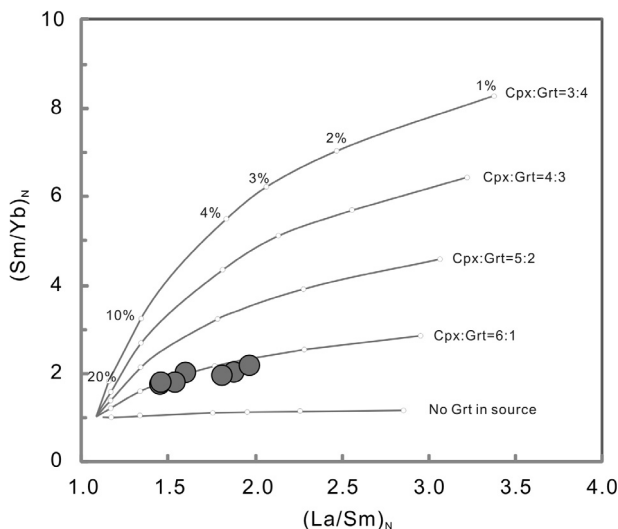


Fig. 8. $(\text{Sm}/\text{Yb})_n$ vs. $(\text{La}/\text{Sm})_n$ diagram for the Xiaoxiaoliu basalts, showing batch melting trends at varying clinopyroxene (Cpx):garnet (Grt) ratios in the residual solid, based on D'Orazio et al. (2001) and Xu et al. (2008).

westward-subducted oceanic crustal material, as discussed above. This inference, combined with the close temporal and spatial links between the basalts and the widespread Cu-bearing porphyritic magmatism within the SYA, is also consistent with a slab tear or break-off model. The Late Triassic geological, geochronological, and geochemical data for the SYA are also consistent with the slab tear or breakoff model outlined by Davies and von Blankenburg (1995), as follows: (1) the presence of bimodal magmatism (basalts and andesite-dacite units, including felsic intrusions), and (2) the presence of a Late Triassic basin in the northern and middle parts of the Yidun arc. However, the restricted distribution of the E-MORE-like basaltic magmatism and associated porphyry Cu deposits to a narrow region within the SYA instead of the whole Yidun arc (Hou et al., 2004), as well as the timing of the magmatism and porphyry Cu formation in the SYA (221–211 Ma), is in keeping with slab tearing rather than breakoff.

5.3. Implications for the generation of porphyry Cu deposits

The separation of the Garze-Litang oceanic basin from the western margin of the Yangtze Craton during the Permian caused

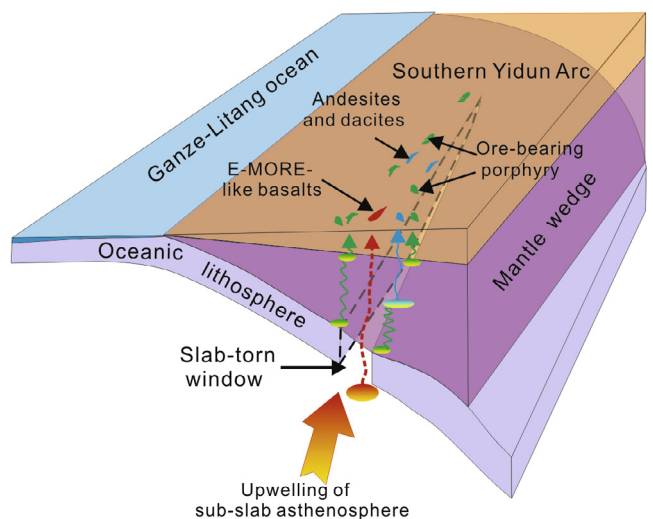


Fig. 9. Simple slab-tear model for westward subduction of the Garze-Litang Ocean and associated Late Triassic magmatism within the southern Yidun arc.

spatial changes in the angle of slab subduction beneath the Yidun arc, including the development of northern high-angle and southern low-angle subduction along the arc (Hou et al., 2004). The former caused partial melting of an area of mantle wedge that was metasomatized during interaction with subduction-derived material, generating the parental magmas of the Triassic non-porphyry-related basalts and andesites of the northern Yidun arc (Hou et al., 2004; Wang et al., 2013). However, low-angle subduction beneath the SYA led to tearing of the slab during the Late Triassic, causing an upwelling of asthenospheric material. This in turn generated the parental magmas of basalts and the formation of associated porphyry Cu deposits within the SYA, as follows (Fig. 9): (1) decompression melting of the upwelling asthenospheric mantle along a tear-related slab window, generating low-K basaltic magmas with E-MORB-like characteristics in the Xiaoxiaoliu area and other parts of the region; (2) partial melting of the edge of the torn slab, generating melts with adakitic affinities; and (3) the interaction and/or mixing of the upwelling melts with melts derived from a mantle wedge that was metasomatized during interaction with subduction-related fluids and sediments. These melts subsequently underwent melting-assimilation-storage-homogenization (MASH) processes beneath the lower crust, forming the paren-

tal magmas of the andesites and dacites in the study area with arc-like characteristics such as HFSE depletions (e.g., Nb and Ta), which in turn formed the parental magmas of the intrusions associated with porphyry Cu deposits. Thus, the formation of a porphyry Cu deposit, at least in the case of the SYA, may require slab-tear and the associated triggered upwelling of asthenospheric mantle material during subduction. We conclude that slab-tear and triggered upwelling of asthenospheric mantle material is one of the most likely mechanisms to produce a porphyry Cu deposit in an active continental margin setting. Similar observations in other oceanic and/or continental lithosphere subduction zones, such as porphyry Cu mineralization on Java Island (Setijadji et al., 2006), within the Luzon Arc (Polve et al., 2007; Fan et al., 2015), in the Canadian Cordillera (Logan and Mihalynuk, 2014), in California and Nevada (du Bray et al., 2014), in the Kerman area of Iran (Shafiei et al., 2009) and in southern Tibet in China (Hou et al., 2006), all suggest that slab tearing is an important process in the generation of porphyry Cu mineralization.

6. Conclusions

- (1) The E-MORB-like geochemical characteristics of the Xiaoxiaoliu basalts suggest they were derived from asthenospheric mantle at ~217 Ma.
- (2) The small volumes of basalt lavas, combined with widespread andesitic-dacitic (including felsic intrusions) magmatism and associated porphyry Cu deposits within the SYA, were most likely generated by Late Triassic tearing of the slab of the westward-dipping Garze-Litang Ocean crust.

Acknowledgements

We are grateful to the Chief Editor Franco Pirajno, the Guest Editor Jun Deng, and two anonymous reviewers for their kind and critically constructive comments and suggestions, which greatly improved the quality of our manuscript. This research was supported by the Major State Basic Research Program of the People's Republic of China (grant number 2015CB452602), the Strategic Priority Research Program (B) of the Chinese Academy of Sciences (XDB03010300), the National Key Research and Development Project of China (2016YFC0600305), the China Geological Survey Project (1212011020000150011), and the Natural Science Foundation of China (41373030, 41573024). This is GIGCAS contribution No. IS-2328.

References

- Bureau of Geology Mineral Resources of Sichuan Province (BGMRSP), 1991. Regional Geology of Sichuan Province. Geological Publishing House, Beijing, pp. 730 (in Chinese with English abstract).
- Chen, J.L., Xu, J.F., Wang, B.D., Kang, Z.Q., Li, J., 2010. Origin of Cenozoic alkaline potassic volcanic rocks at KonglongXiang, Lhasa terrane, Tibetan Plateau: products of partial melting of a mafic lower-crustal source. *Chem. Geol.* 273, 286–299.
- Chen, J.L., Xu, J.F., Ren, J.B., Huang, X.X., Wang, B.D., 2014. Geochronology and geochemical characteristics of Late Triassic porphyritic rocks from the Zhongdian arc, eastern Tibet, and their tectonic and metallogenetic implications. *Gondwana Res.* 26, 292–504.
- Condie, K.C., 2003. Incompatible element ratios in oceanic basalts and komatiites, tracking deep mantle sources and continental growth rates with time. *Geochim. Geophys. Geosyst.* 4 (1), 1005. <http://dx.doi.org/10.1029/2002GC000333>.
- Davies, J.H., von Blankenburg, F., 1995. Slab breakoff: a model of lithospheric detachment and its test in the magmatism and deformation of collisional orogens. *Earth Planet. Sci. Lett.* 129, 85–102.
- Defant, M.J., Drummond, M.S., 1990. Derivation of some modern arc magmas by melting of young subducted lithosphere. *Nature* 347, 662–665.
- Deng, J., Wang, Q.F., Li, G.J., Li, C.S., Wang, C.M., 2014. Tethys tectonic evolution and its bearing on the distribution of important mineral deposits in the Sanjiang region, SW China. *Gondwana Res.* 26, 419–437.
- D'Orazio, M., Agostini, S., Innocenti, F., Haller, M.J., Manetti, P., Mazzarini, F., 2001. Slab windowrelated magmatism from southernmost South America: the Late Miocene mafic volcanics from the Estancia Glencross Area (~52 S, Argentina–Chile). *Lithos* 57, 67–89.
- du Bray, E.A., John, D.A., Cousens, B.L., 2014. Petrologic, tectonic, and metallogenetic evolution of the southern segment of the ancestral Cascades magmatic arc, California and Nevada. *Geosphere* 10, 1–39.
- Fan, J.K., Wu, S.G., Spence, G., 2015. Tomographic evidence for a slab tear induced by fossil ridge subduction at Manila Trench, South China Sea. *Int. Geol. Rev.* 57, 998–1013.
- Fitton, J.G., 1995. Coupled molybdenum and niobium depletion in continental basalts. *Earth Planet. Sci. Lett.* 136, 715–721.
- Goto, A., Tatsumi, Y., 1996. Quantitative analyses of rock samples by an X-ray fluorescence spectrometer (II). *Rigaku J.* 13, 20–39.
- Green, D.H., 1976. Experimental testing of "equilibrium" partial melting of peridotite under water-saturated, high-pressure conditions. *Can. Mineral.* 14, 255–268.
- Hofmann, A.W., 1997. Mantle geochemistry: the message from oceanic volcanism. *Nature* 385, 219–229.
- Hofmann, A.W., 2014. Sampling mantle heterogeneity through oceanic basalts: Isotopes and trace elements. In: Holland, H.D., Turekian, K.K. (Eds.), Treatise on Geochemistry, 2nd edn., vol. 3 Elsevier, Oxford, pp. 67–101. <http://dx.doi.org/10.1016/B978-0-08-095975-7.00203-5>.
- Hou, Z.Q., Zhang, H.R., 2015. Geodynamics and metallogenesis of the eastern Tethyan metallogenetic domain. *Ore Geol. Rev.* 70, 346–384.
- Hou, Z.Q., Yang, Y.Q., Qu, X.M., Huang, D.H., Lv, Q.T., Wang, H.P., Yu, J.J., Tang, S.H., 2004. Tectonic evolution and mineralization systems of the Yidun arc orogen in Sanjiang region, China. *Acta Geol. Sin.* 78, 109–120.
- Hou, Z.Q., Zhao, Z.D., Gao, Y.F., Yang, Z.M., Jiang, W., 2006. Tearing and dischronal subduction of the Indian continental slab: Evidence form Cenozoic Gangdese volcano-magmatic rocks in south Tibet. *Acta Petrol. Sin.* 22, 761–774 (in Chinese with English abstract).
- Houseman, G.A., McKenzie, D.P., Molnar, J., 1981. Convective instability of a thickened boundary layer and its relevance for the thermal evolution of continental convergent belts. *J. Geophys. Res.* 86, 6115–6132.
- Huang, X.X., 2013. Geochronology, Geochemistry and Petrogenesis of Indosinian and Yanshanian Igneous Rocks in Zhongdian Arc (MD thesis of the Graduate School of Chinese Academy of Sciences). 90 (in Chinese with English abstract).
- Kay, S.M., Mpodozis, C., 2001. Central Andean ore deposits linked to evolving shallow subduction systems and thickening crust. *GSA Today* 11 (3), 4–9.
- Kelemen, P.B., Yogodzinski, G.M., Scholl, D.W., 2003. Along-strike variation in the Aleutian Island Arc: genesis of high Mg# andesite and implications for continental crust. In: Eiler, J. (Ed.), Inside the Subduction Factory, 138. AGU Monogr., pp. 223–276.
- Li, X.H., McCulloch, M.T., 1998. Geochemical characteristics of Cretaceous mafic dikes from Northern Guangdong, SE China: age, origin and tectonic significance. In: Flower, M.F.J. (Ed.), Mantle Dynamics and Plate Interactions in East Asia Geodynamics, 27. AGU Monogr., pp. 405–419.
- Li, X.H., Liu, D.Y., Sun, M., Li, W.X., Liang, X.R., Liu, Y., 2004. Precise Sm–Nd and U–Pb isotopic dating of the super-giant Shizhu Yuan polymetallic deposit and its host granite, Southeast China. *Geol. Mag.* 141, 225–231.
- Li, X.H., Liu, Y., Li, Q.L., Guo, C.H., Chamberlain, K.R., 2009. Precise determination of Phanerozoic zircon Pb/Pb age by multi-collector SIMS without external standardization. *Geochim. Geophys. Geosyst.* 10, Q04010. <http://dx.doi.org/10.1029/c002400>.
- Li, X.H., Li, W.X., Wang, X.C., Li, Q.L., Liu, Y., Tang, G.Q., Gao, Y.Y., Wu, F.Y., 2010. SIMS U–Pb zircon geochronology of porphyry Cu–Au–(Mo) deposits in the Yangtze River Metallogenic Belt, eastern China: magmatic response to early Cretaceous lithospheric extension. *Lithos* 119, 427–438.
- Logan, J.M., Mihalynuk, M.G., 2014. Tectonic controls on Early Mesozoic paired alkaline porphyry deposit belt (Cu–Au ± Ag–Pt–Pd–Mo) within the Canadian Cordillera. *Econ. Geol.* 109, 827–858.
- Ludwig, K.R., 2001. Users Manual for Isoplots/Ex rev. 2.49. Berkeley Geochronology Centre Special Publication. No. 1a, pp. 56.
- Martin, H., Smithies, R.H., Rapp, R., Moyen, J.F., Champion, D., 2005. An overview of adakite, tonalit-trondhjemite-granodiorite (TTG), and sanukitoid: relationships and some implications for crustal evolution. *Lithos* 79, 1–24.
- McKenzie, D.P., O'Nions, R.K., 1991. Partial melt distributions from inversion of rare earth element concentrations. *J. Petrol.* 32, 1021–1091.
- Pearce, J.A., 1982. Trace element characteristics of lavas from destructive plate boundaries. In: Thorpe, R.S. (Ed.), Andesites. John Wiley, New York, pp. 525–548.
- Pearce, J.A., 2008. Geochemical fingerprinting of oceanic basalts with applications to ophiolite classification and the search for Archean oceanic crust. *Lithos* 100, 14–48.
- Plank, T., Langmuir, C.H., 1998. The chemical composition of subducting sediment and its consequences for the crust and mantle. *Chem. Geol.* 145, 325–394.
- Polve, M., Maury, R.C., Jego, S., Bellon, H., Margoum, A., Yumul Jr, G.P., Payot, B.D., Tamayo Jr., R.A., Cotten, J., 2007. Temporal geochemical evolution of Neogene magmatism in the Baguio Gold-Copper mining district (Northern Luzon, Philippines). *Resour. Geol.* 57, 197–218.
- Reid, A.J., Wilson, C.J.L., Liu, S., 2005. Structural evidence for the Permo-Triassic tectonic evolution of the Yidun Arc, eastern Tibetan plateau. *J. Struct. Geol.* 27, 119–137.
- Ren, J.B., Xu, J.F., Chen, J.L., 2011. Zircon geochronology and geological implications of ore-bearing porphyries from Zhongdian arc. *Acta Petrol. Sin.* 27, 2591–2599.

- Robinson, J.A., Wood, B.J., 1998. The depth of the spinel to garnet transition at the peridotite solidus. *Earth Planet. Sci. Lett.* 164, 277–284.
- Roger, F., Jolivet, M., Malavielle, J., 2010. The tectonic evolution of the Songpan-Garze (North Tibet) and adjacent areas from Proterozoic to present: a synthesis. *J. Asian Earth Sci.* 39, 254–269.
- Rudnick, R., Gao, S., 2003. Composition of the continental crust. In: Rudnick, R.L. (Ed.), *The Crust*, vol. 3. Elsevier-Pergamon, Oxford, pp. 1–64. Treatise on Geochemistry (Holland, H.D., Turekian, K.K. (Eds.)).
- Schilling, J.G., 1973. Iceland mantle plume: geochemical study of the Reykjanes Ridge. *Nature* 242, 565–571.
- Setijadji, L.D., Kajino, S., Imai, A., Watanabe, K., 2006. Cenozoic island arc magmatism in Java Island (Sunda Arc, Indonesia): clues on relationships between geodynamics of volcanic centers and ore mineralization. *Resour. Geol.* 56, 267–292.
- Shafeei, B., Haschke, M., Shahabpour, J., 2009. Recycling of orogenic arc crust triggers porphyry Cu mineralization in Kerman Cenozoic arc rocks, southeastern Iran. *Mineral. Deposita* 44, 265–283.
- Stacey, J.S., Kramers, J.D., 1975. Approximation of terrestrial lead isotope evolution by a two-stage model. *Earth Planet. Sci. Lett.* 26, 207–221.
- Sun, S.S., McDonough, W.F., 1989. Chemical and isotopic systematics of oceanic basalts: implications for mantle composition and processes. In: Saunders, A.D., Norry, M.J. (Eds.), *Magmatism in the Ocean Basins*, vol. 42. Geol. Soc. Spec. Pub., pp. 313–345.
- Thompson, R.N., Morrison, M.A., 1988. Asthenospheric and lowerlithospheric mantle contributions to continental extensional magmatism: an example from the British tertiary province. *Chem. Geol.* 68, 1–15.
- Ulrich, M., Hémond, C., Nonnotte, P., Jochum, K.P., 2012. OIB/seamount recycling as a possible process for E-MORB genesis. *Geochem. Geophys. Geosyst.* 13 (6). doi.org/10.1029/2012GC004078.
- Wang, B.Q., Zhou, M.F., Li, J.W., Yan, D.P., 2011. Late Triassic porphyritic intrusions and associated volcanic rocks from the Shangri-La region, Yidun terrane, Eastern Tibetan Plateau: adakitic magmatism and porphyry copper mineralization. *Lithos* 127, 24–38.
- Wang, B.Q., Zhou, M.F., Gao, J.F., Yan, D.P., 2013. Petrogenesis and tectonic implications of the Triassic volcanic rocks in the northern Yidun Terrane, Eastern Tibet. *Lithos* 175–176, 285–301.
- Wang, X.S., Bi, X.W., Leng, C.B., Zhong, H., Tang, H.F., Chen, W., Yin, G.H., Huang, D.Z., Zhou, M.F., 2014. Geochronology and geochemistry of Late Cretaceous igneous intrusions and Mo-Cu-(W) mineralization in the southern Yidun Arc, SW China: implications for metallogenesis and geodynamic setting. *Ore Geol. Rev.* 61, 73–95.
- Wanke, M., Portnyagin, M., Hoernle, K., Reinhard Werner, R., Folkmar Hauff, F., Paul van den Boogaard, P., Garbe-Schönberg, D., 2012. Bowers Ridge (Bering Sea): an Oligocene-Early Miocene island arc. *Geology* 40, 687–690.
- Wei, G.J., Liang, X.R., Li, X.H., Liu, Y., 2002. Precise measurement of Sr isotopic composition of liquid and solid base using (LP) MC-ICPMS. *Geochimica* 31, 295–299.
- White, W.M., Hofmann, A.W., 1982. Sr and Nd isotope geochemistry of oceanic basalts and mantle evolution. *Nature* 291, 821–825.
- Wiedenbeck, M., Alle, P., Corfu, F., Griffin, W.L., Meier, M., Oberli, F., Vonquadt, A., Roddick, J.C., Speigel, W., 1995. Three natural zircon standards for U-Th–Pb, Lu–Hf, trace-element and REE analyses. *Geostand. Newsl.* 19, 1–23.
- Willbold, M., Stracke, A., 2006. Trace element composition of mantle end members: implications for recycling of oceanic and upper and lower continental crust. *Geochem. Geophys. Geosyst.* 7, Q04004. 10.1029 /2005GC001005.
- Winchester, J.A., Floyd, P.A., 1977. Geochemical magma type discrimination: application to altered and metamorphosed basic igneous rocks. *Earth Planet. Sci. Lett.* 28, 459–469.
- Wood, D.A., 1980. The application of a Th-Hf-Ta diagram to problems of tectonomagmatic classification and to establishing the nature of crustal contamination of basaltic lavas of the British Tertiary Volcanic Province. *Earth Planet. Sci. Lett.* 50, 11–30.
- Xu, J.F., Castillo, P.R., Li, X.H., Yu, X.Y., Zhang, B.R., Han, Y.W., 2002. MORB-type rocks from the Paleo-Tethyan Mian-Lueyang northern ophiolite in the Qinling Mountains, central China: implications for the source of the low $^{206}\text{Pb}/^{204}\text{Pb}$ and high $^{143}\text{Nd}/^{144}\text{Nd}$ mantle component in the Indian Ocean. *Earth Planet. Sci. Lett.* 198, 323–337.
- Xu, Y.G., Lan, J.B., Yang, Q.J., Huang, X.L., Qiu, H.N., 2008. Eocene breakoff of the Neo-Tethyan slab as inferred from intraplate-type mafic dykes in the Gaoligong orogenic belt, eastern Tibet. *Chem. Geol.* 255, 439–453.
- Yan, Q.R., Wang, Z.Q., Liu, S.W., Li, Q.G., Zhang, H.Y., Wang, T., Liu, D.Y., Shi, Y.R., Jian, P., Wang, J.G., Zhang, D.H., Zhao, J., 2005. Opening of the Tethys in southwest China and its significance to the breakup of East Gondwanaland in Late Paleozoic: evidence from SHRIMP U-Pb zircon analyses for the Garze ophiolite block. *Chin. Sci. Bull.* 50, 256–264.
- Yang, T.N., Hou, Z.Q., Wang, Y., Zhang, H.R., Wang, Z.L., 2012. Late Paleozoic to Early Mesozoic tectonic evolution of northeast Tibet: evidence from the Triassic composite western Jinsha-Garzé-Litang suture. *Tectonics* 31 (TC4004), 2012. http://dx.doi.org/10.1029/2011TC003044.
- Yogodzinski, G.M., Lees, J.M., Churikova, T.G., Dorendorf, F., Woerner, G., Volynets, O.N., 2001. Geochemical evidence for the melting of subducting oceanic lithosphere at plate edges. *Nature* 409, 500–504.
- Zindler, A., Hart, S., 1986. Chemical geodynamics. *Annu. Rev. Earth Planet. Sci.* 14, 493–571.
- Zu, B., Xue, C.J., Chi, G.X., Zhao, X.B., Li, C., Zhao, Y., Yalikum, Y., Zhang, G.Z., Zhao, Y., 2016. Geology, geochronology and geochemistry of granitic intrusions and the related ores at the Hongshan Cu-polymetallic deposit: Insights into the Late Cretaceous post-collisional porphyry-related mineralization systems in the southern Yidun arc, SW China. *Ore Geol. Rev.* 77, 25–42.